Journal of the Brazilian Society of Mechanical Sciences and Engineering (2020) 42:263
https://doi.org/10.1007/s40430-020-02328-z

TECHNICAL PAPER

Estimation of slip flow parameters in microscale conjugated heat transfer problems

Géssica R. Silva[1] · Diego C. Knupp[1] · Carolina P. Naveira-Cotta[2] · Renato M. Cotta[2,3] · Antônio J. Silva Neto[1]

Received: 22 October 2019 / Accepted: 30 March 2020 / Published online: 28 April 2020

Abstract

In this work, it is proposed the direct and inverse analyses of the forced convection of an incompressible gas flow within rectangular channels in the range of the slip flow regime by taking into account the wall conjugation and the axial conduction effects. The Generalized Integral Transform Technique (GITT) combined with the single-domain reformulation strategy is employed in the direct problem solution of the three-dimensional steady forced convection formulation. A non-classical eigenvalue problem that automatically accounts for the longitudinal diffusion operator is here proposed. The Bayesian framework implemented with the maximum a posteriori objective function is used in the formulation of the inverse problem, whose main objective is to estimate the temperature jump coefficient, the velocity slip coefficient, and the Biot number, using only external temperature measurements, as obtained, for instance, with an infrared measurement system. A comprehensive numerical investigation of possible experimental setups is performed in order to verify the influence of the Biot number, wall thickness, and Knudsen number on the precision of the unknown parameters estimation.

Keywords Conjugated problem · Slip flow · Temperature jump · Generalized Integral Transform Technique · Single-domain formulation · Internal convection · Bayesian inference

List of symbols

Bi	Biot number
CI_i	Relative measure of the confidence interval of the estimated value $\hat{P}_i$
D_h	Hydraulic diameter
h_e	Convective heat transfer coefficient
$\mathbf{J}$	Jacobian matrix
$\mathcal{J}$	Scaled sensitivity coefficients
k	Thermal conductivity
K	Dimensionless thermal conductivity
Kn	Knudsen number
L_x	Distance from the channel centerline to the external face of the channel wall (x direction)
L_y	Distance from the channel centerline to the external face of the channel wall (y direction)
M	Truncation order of the eigenfunction expansion (eigenvalue problem solution)
N	Truncation order of the temperature eigenfunction expansion
n	Norm of the eigenfunction $\psi(X, Y)$
N_p	Dimension of the vector $\mathbf{P}$
N_d	Dimension of the vector $\mathbf{Y}$
$\mathbf{n}$	Outward-drawn normal vector
$\mathbf{P}$	Vector of parameters
$\mathbf{P}_{\mathrm{exact}}$	Vector with the exact values of the sought parameters
Pe	Péclet number
Pr	Prandtl number
Re	Reynolds number
S	Objective function
T	Temperature
T_∞	Ambient temperature

Technical Editor: Francis HR Franca, Ph.D.

✉ Diego C. Knupp
diegoknupp@iprj.uerj.br

[1] LEMA - Laboratory of Experimentation and Numerical Simulation in Heat and Mass Transfer, Department of Mechanical Engineering and Energy, Polytechnic Institute, Rio de Janeiro State University, IPRJ/UERJ, Rua Bonfim 25, Vila Amelia, Nova Friburgo, RJ 28625-570, Brazil

[2] LabMEMS - Laboratory of Nano and Microfluidics and Microsystems, Mechanical Engineering Department - PEM, POLI/COPPE, Federal University of Rio de Janeiro, UFRJ, Cx. Postal 68503, Rio de Janeiro, RJ 21945-970, Brazil

[3] Present Address: General Directorate of Nuclear and Technological Development, DGDNTM, Brazilian Navy, Ministry of Defense, Brasilia, Brazil

u	Fully developed flow velocity
U	Dimensionless flow velocity
$\mathbf{V}$	Covariance matrix of the prior information
$\mathbf{W}$	Covariance matrix of the experimental errors
y	Transversal coordinate
X, Y	Dimensionless transversal coordinates
$\mathbf{Y}$	Vector of temperature measurements
z	Longitudinal coordinate
Z	Dimensionless longitudinal coordinate
Z_f	Dimensionless channel length

Greek symbols

α_f	Thermal diffusivity of the fluid
α_m	Tangential momentum accommodation coefficient
α_t	Thermal accommodation coefficient
β	General temperature jump coefficient in the 3D formulation
β_t	Wall temperature jump coefficient
β_v	Wall velocity slip coefficient
ϵ_{fic}	Dimensionless thickness of the fictitious layer
γ	Specific heat ratio
λ	Molecular mean free path
Ω	Auxiliary eigenfunctions
ω	Eigenvalue corresponding to the eigenfunction Ω
ψ	Temperature eigenfunctions
η	Eigenvalue corresponding to the eigenfunction ψ
$\boldsymbol{\mu}$	Mean vector of the prior density
π	Probability density function
σ_e	Standard deviation of the experimental errors
σ_{P_i}	Standard deviation of the estimated parameter P_i
θ	Dimensionless temperature
ν	Kinematic viscosity

Subscripts and superscripts

ac	Quantity corresponding to the axial conduction term
av	Average
f	Fluid flow region
fic	Quantity corresponding to the fictitious layer
in	Quantity corresponding to the entrance of the channel
int	Interface position
i, j, m, n	Indices
s	Solid region (channel walls)
w	Quantity corresponding to the external face of the channel wall
X	Quantity corresponding to the X direction
Y	Quantity corresponding to the Y direction
*	Domain including the fictitious layer
ˆ	Estimated value
+	Upper bound of the confidence interval
−	Lower bound of the confidence interval

1 Introduction

Over the last few decades, a huge effort has been devoted toward miniaturization of thermomechanical equipment, aiming at devices with improved thermal efficiency and overall performance [1]. A number of published contributions addressing the formulation and solution of heat and fluid flow problems at the microscale were directed to the understanding of discrepancies observed between microscale experimental results and macroscale correlations and simulations [2]. These discrepancies are mainly due to scaling effects, such as entrance effects, conjugated heat transfer, viscous heating, electric double-layer (EDL) effects, temperature-dependent properties, surface roughness, rarefaction, and compressibility effects. These phenomena, often negligible in macroscale problems, may have a significant influence and have to be accounted for when dealing with heat and fluid flow in microsystems [3].

Among different model modifications proposed to describe more adequately the fluid flow and heat transfer in microchannels, the consideration of slip flow in opposition to the classical no-slip condition has been the subject of numerous investigations [4] and has been handled both analytically and numerically in previous works for different microchannel geometries, such as circular microtubes [5–10] and rectangular and parallel plate microchannels [11–17]. Also of major relevance in improving theoretical predictions of heat transfer in microsystems is the consideration of conjugated conduction–convection heat transfer to accurately describe the thermal effects of the solid substrate that comprises the microsystem walls, as can be seen in [14, 18–20].

Recently, Knupp et al. [14] proposed a single-domain formulation strategy in combination with the Generalized Integral Transform Technique (GITT). This methodology allows for heterogeneous multi-region problems to be written as single-domain formulations by making use of spatially variable coefficients with abrupt transitions occurring at the interfaces and was successfully employed in the solution of different conjugated heat transfer problems [21–25]. This strategy was then improved in order to deal with conjugated conduction–convection heat transfer for incompressible laminar gas flow in microchannels, within the range of validity of the slip flow regime, in which velocity slip and temperature jump at the wall play a major role in heat transfer. As the single-domain formulation satisfies the temperature continuity at the interfaces, the authors proposed the introduction of a fictitious layer between the fluid region and the channel wall, in order to impose the desired thermal resistance between the fluid and the wall, modeling the temperature jump at the solid–fluid interface [26].

The accurate simulation of such problems is, however, dependent on an accurate determination of the momentum and thermal accommodation coefficients, required by the slip and temperature jump boundary conditions provided by the slip flow model that accounts for non-continuum effects at the fluid–surface interactions [4]. Some experimental works are available in the literature regarding measurements of the tangential momentum accommodation coefficient [27], showing its dependency on the surface cleanliness and roughness, but few results are available regarding the measurement of the thermal accommodation coefficient [28]. Sharipov [29] presents a critical review of theoretical and experimental data on the momentum and thermal accommodation coefficients within the open literature, and the author emphasizes that apparently no experimental data on the thermal accommodation coefficient in actual heat and fluid flow conditions pertinent to microsystems applications are available. Some theoretical results for the estimation of the thermal accommodation coefficient are available [30–32], but specific aspects commonly present in microflows are generally neglected, such as the wall conjugation effects and/or the presence of axial conduction due to low Péclet numbers.

This work is aimed at performing an inverse analysis of forced convection in rectangular microchannels with slip flow via integral transforms and Bayesian inference, extending the study performed in Refs. [31, 32] in order to take into account important microscale effects, such as wall conjugation and axial conduction. The GITT is employed in combination with the single-domain reformulation to offer a hybrid numerical–analytical solution to the three-dimensional steady forced convection formulation. A non-classical eigenvalue problem is proposed that directly incorporates the effect of the longitudinal heat diffusion term. A Bayesian framework is adopted for the inverse problem formulation and solution, here implemented with the minimization of the maximum a posteriori (MAP) objective function, in order to take advantage of prior information generally available for the tangential momentum accommodation coefficient and the external wall Biot number. The limiting situation of a rectangular channel with high aspect ratio is then considered for numerical computations, so as to reduce the number of parameters in the inverse problem analysis. A critical analysis on possible experimental setups is performed in order to identify a favorable scenario for the estimation of the thermal accommodation coefficient, employing only external temperature measurements along the channel walls.

2 Direct problem formulation and solution methodology

Consider steady-state incompressible gas flow in a rectangular channel, undergoing internal forced convective heat transfer. The external faces of the channel walls exchange heat with the surrounding environment at a different temperature from the inlet gas temperature. The channel walls are considered to participate in the heat transfer process through axial and transversal heat conduction. The dimensionless formulation of this problem, considering the first-order slip flow modeling [33], can be written as follows, for the fluid region:

$$\begin{aligned} U_f(X,Y)\frac{\partial \theta_f(X,Y,Z)}{\partial Z} &= \left(\frac{D_h}{L_x}\right)^2 \frac{\partial^2 \theta_f}{\partial X^2} \\ &+ \left(\frac{D_h}{L_y}\right)^2 \frac{\partial^2 \theta_f}{\partial Y^2} + \frac{1}{\mathrm{Pe}^2}\frac{\partial^2 \theta_f}{\partial Z^2}, \\ &\text{in } -X_{\mathrm{int}} \le X \le X_{\mathrm{int}}, -Y_{\mathrm{int}} \le Y \le Y_{\mathrm{int}}, 0 \le Z \le Z_f \end{aligned} \tag{1a}$$

with the following boundary conditions:

$$\theta_f(X,Y,0) = 1, \quad \left.\frac{\partial \theta_f}{\partial Z}\right|_{Z=Z_f} = 0 \tag{1b}$$

and the following interface conditions, considering temperature jump:

$$\begin{aligned} &\frac{D_h}{L_x}\beta_t \mathrm{Kn}\frac{\partial \theta_f}{\partial \mathbf{n}} + \theta_f(X,Y,Z) = \theta_s(X,Y,Z), \\ &\text{for } X = -X_{\mathrm{int}}, \text{ and } X = X_{\mathrm{int}} \end{aligned} \tag{1c}$$

$$\begin{aligned} &\frac{D_h}{L_y}\beta_t \mathrm{Kn}\frac{\partial \theta_f}{\partial \mathbf{n}} + \theta_f(X,Y,Z) = \theta_s(X,Y,Z), \\ &\text{for } Y = -Y_{\mathrm{int}}, \text{ and } Y = Y_{\mathrm{int}} \end{aligned} \tag{1d}$$

The heat conduction problem at the channel walls is given by:

$$\left(\frac{D_h}{L_x}\right)^2 \frac{\partial^2 \theta_s}{\partial X^2} + \left(\frac{D_h}{L_y}\right)^2 \frac{\partial^2 \theta_s}{\partial Y^2} + \frac{1}{\mathrm{Pe}^2}\frac{\partial^2 \theta_s}{\partial Z^2} = 0 \tag{2a}$$

with boundary and interface conditions

$$\theta_s(X,Y,0) = 1, \quad \left.\frac{\partial \theta_s}{\partial Z}\right|_{Z=Z_f} = 0 \tag{2b}$$

$$K_s\frac{\partial \theta_s}{\partial Y} = \frac{\partial \theta_f}{\partial Y}, \text{ at } Y = -Y_{\mathrm{int}} \text{ and } Y = Y_{\mathrm{int}} \tag{2c}$$

$$K_s \frac{\partial \theta_s}{\partial X} = \frac{\partial \theta_f}{\partial X}, \text{ at } X = -X_{\text{int}} \text{ and } X = X_{\text{int}} \tag{2d}$$

$$\frac{\partial \theta_s}{\partial \mathbf{n}} + \text{Bi}_X \theta_s(X, Y, Z) = 0, \text{for } X = -1 \text{ and } X = 1 \tag{2e}$$

$$\frac{\partial \theta_s}{\partial \mathbf{n}} + \text{Bi}_Y \theta_s(X, Y, Z) = 0, \text{for } Y = -1, \text{ and } Y = 1 \tag{2f}$$

where the following dimensionless groups were employed:

$$Z = \frac{z/D_h}{\text{RePr}} = \frac{z}{D_h \text{Pe}}; \tag{3a}$$

$$Y = \frac{y}{L_y}; \tag{3b}$$

$$X = \frac{x}{L_x}; \tag{3c}$$

$$U = \frac{u}{u_{\text{av}}}; \tag{3d}$$

$$\theta = \frac{T - T_\infty}{T_{\text{in}} - T_\infty}; \tag{3e}$$

$$\text{Bi}_X = \frac{h_e L_x}{k_s} \tag{3f}$$

$$\text{Bi}_Y = \frac{h_e L_y}{k_s}; \tag{3g}$$

$$\text{Re} = \frac{u_{\text{av}} D_h}{\nu_f}; \tag{3h}$$

$$\text{Pr} = \frac{\nu_f}{\alpha_f}; \tag{3i}$$

$$\text{Pe} = \text{RePr} = \frac{u_{\text{av}} D_h}{\alpha_f}; \tag{3j}$$

$$\text{Kn} = \frac{\lambda}{D_h}; \tag{3k}$$

$$K = \frac{k}{k_f} \tag{3l}$$

In the solution methodology with the single-domain formulation, this conjugated problem is formulated as a single-region model, accounting for the heat transfer phenomena simultaneously at both the fluid flow and the channel solid walls. This is achieved by making use of coefficients represented as space variable functions where abrupt transitions occur at the fluid–solid wall interfaces. In such approach, the temperature and heat flux continuity across the interfaces are automatically satisfied. In order to extend this methodology to tackle conjugated heat transfer problems within the slip flow regime, Knupp et al. [26] proposed the introduction of a thin fictitious layer of thickness ϵ_{fic}, which is inserted between the fluid region and the channel wall, in order to model the temperature jump at the surface. The representation of the augmented domain with the fictitious layer at the interface is depicted in Fig. 1. The single-domain formulation for the temperature distribution within the augmented domain, $\theta^*(X, Y, Z)$, can be written as:

$$\begin{aligned} U(X,Y)\frac{\partial \theta^*}{\partial Z} &= \frac{\partial}{\partial Y}\left(K(X,Y)\frac{\partial \theta^*}{\partial Y}\right) \\ &+ \frac{\partial}{\partial X}\left(K(X,Y)\frac{\partial \theta^*}{\partial X}\right) + \frac{K_{\text{ac}}(Y)}{\text{Pe}^2}\frac{\partial^2 \theta^*}{\partial Z^2}, \\ &\text{in } -1-\epsilon_{\text{fic}} \le Y \le 1+\epsilon_{\text{fic}}, \quad -1-\epsilon_{\text{fic}} \le X \le 1+\epsilon_{\text{fic}}, \\ &0 \le Z \le Z_f \end{aligned} \tag{4a}$$

with the following boundary conditions at the longitudinal direction:

$$\theta^*(X, Y, 0) = 1, \ \left.\frac{\partial \theta^*}{\partial Z}\right|_{Z=Z_f} = 0 \tag{4b}$$

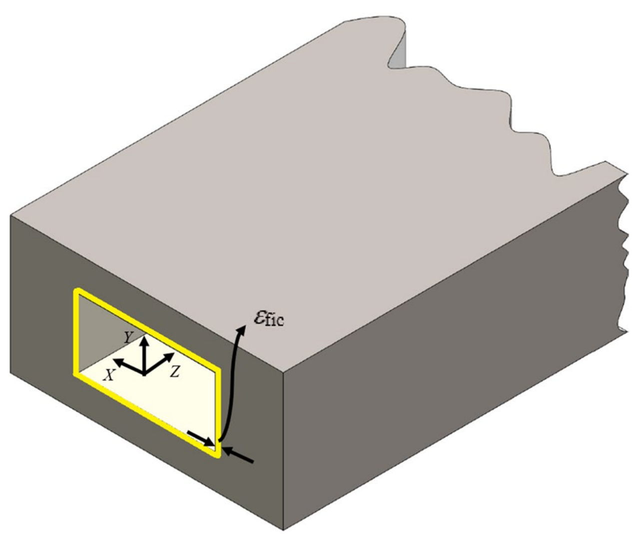

Fig. 1 Schematic representation of the augmented domain with fictitious layer

and the following boundary conditions at the external lateral surfaces:

$$\frac{\partial \theta^*}{\partial \mathbf{n}} + \mathrm{Bi}_X \theta^*(X, Y, Z) = 0, \text{for } X = -1 - \epsilon_{\text{fic}} \text{ and } X = 1 + \epsilon_{\text{fic}} \tag{4c}$$

$$\frac{\partial \theta^*}{\partial \mathbf{n}} + \mathrm{Bi}_Y \theta^*(X, Y, Z) = 0, \text{for } Y = -1 - \epsilon_{\text{fic}} \text{ and } Y = 1 + \epsilon_{\text{fic}} \tag{4d}$$

where

$$U(X, Y) = \begin{cases} U_f(X, Y), & \text{in fluid region} \\ 0, & \text{in solid region} \end{cases} \tag{4e}$$

$$K(X, Y) = \begin{cases} 1, & \text{in fluid region} \\ K_{\text{fic}}, & \text{in fictitious layer} \\ K_s, & \text{in solid region} \end{cases} \tag{4f}$$

$$K_{\text{ac}}(X, Y) = \begin{cases} 1, & \text{in fluid region} \\ 0, & \text{in fictitious layer} \\ K_s, & \text{in solid region} \end{cases} \tag{4g}$$

If the flow is considered fully developed, which is quite feasible due to the typical low Reynolds numbers in micro-scale applications, the velocity field $U_f(X, Y)$ can be readily calculated in terms of the slip velocity coefficient and the Knudsen number [11]. The thermal conductivity of the fictitious layer, K_{fic}, is responsible for imposing the desired thermal resistance across the fictitious layer, hence modeling the desired temperature jump. It should be noticed that the fictitious layer is modeled in order to impose a thermal resistance in the transversal direction only, simulating the temperature jump, with no effects on the longitudinal direction. Hence, it is considered that the heat conduction in this region occurs through the transversal direction only, and hence K_{ac}=0 within the fictitious layer. This formulation can be solved via separation of variables, yielding the following eigenfunction expansion for the temperature field:

$$\theta^*(X, Y, Z) = \sum_{i=1}^{N} C_i e^{-\eta_i^2 Z} \psi_i(X, Y) \tag{5}$$

where the eigenfunctions and eigenvalues, given by $\psi_i(X, Y)$ and η_i, respectively, come from a non-classical eigenvalue problem which incorporates the axial conduction term:

$$\nabla \cdot \big(K(X, Y)\nabla\psi_i(X, Y)\big) + [K_{\text{ac}}(X, Y)\eta_i^4 + U(X, Y)\eta_i^2]\psi_i(X, Y) = 0, \\ \text{in } -1 - \epsilon_{\text{fic}} \le Y \le 1 + \epsilon_{\text{fic}}, \quad -1 - \epsilon_{\text{fic}} \le X \le 1 + \epsilon_{\text{fic}} \tag{6a}$$

with boundary conditions

$$\frac{\partial \psi_i}{\partial \mathbf{n}} + \mathrm{Bi}_X \psi_i(X, Y) = 0, \text{for } X = -1 - \epsilon_{\text{fic}}, \text{ and } X = 1 + \epsilon_{\text{fic}} \tag{6b}$$

$$\frac{\partial \psi_i}{\partial \mathbf{n}} + \mathrm{Bi}_Y \psi_i(X, Y) = 0, \text{for } Y = -1 - \epsilon_{\text{fic}} \text{ and } Y = 1 + \epsilon_{\text{fic}} \tag{6c}$$

This non-classical eigenvalue problem does not allow for an explicit analytic solution, but the generalized integral transform technique can be used in order to provide a hybrid numerical–analytical solution constructed upon a simpler auxiliary eigenvalue problem, with explicit analytical solution. We first consider the proposition of the following integral transform pair:

$$\text{transform: } \bar{\psi}_{i,n} = \int_V U(X, Y)\Omega_n(X, Y)\psi_i(X, Y)dV \tag{7a}$$

$$\text{inverse: } \psi_i(X, Y) = \sum_{n=1}^{\infty} \Omega_n(X, Y)\bar{\psi}_{i,n} \tag{7b}$$

where the eigenfunctions $\Omega_n(X, Y)$ and the corresponding eigenvalues ω_n come from a simpler auxiliary eigenvalue problem. In this work, we have chosen the simplest possible auxiliary problem, given by:

$$\nabla^2\Omega_n(X, Y) + \omega_n^2\Omega_n(X, Y) = 0, \\ \text{in } -1 - \epsilon_{\text{fic}} \le Y \le 1 + \epsilon_{\text{fic}}, \quad -1 - \epsilon_{\text{fic}} \le X \le 1 + \epsilon_{\text{fic}} \tag{8a}$$

$$\frac{\partial \Omega_n}{\partial \mathbf{n}} + \mathrm{Bi}_X \Omega_n(X, Y) = 0, \text{for } X = -1 - \epsilon_{\text{fic}}, \text{ and } X = 1 + \epsilon_{\text{fic}} \tag{8b}$$

$$\frac{\partial \Omega_n}{\partial \mathbf{n}} + \mathrm{Bi}_Y \Omega_n(X, Y) = 0, \text{for } Y = -1 - \epsilon_{\text{fic}} \text{ and } Y = 1 + \epsilon_{\text{fic}} \tag{8c}$$

Then, Eq. (6a) is operated on with $\int_V \Omega_n(X, Y)(\cdot)dV$, to yield the following algebraic system in a matrix form:

$$(\mathbf{A} + \mathbf{C})\{\bar{\psi}\} = (\eta^4\mathbf{E} + \eta^2\mathbf{B})\{\bar{\psi}\} \tag{9a}$$

where the elements of the corresponding coefficient matrices are given by

$$a_{mn} = \int_V \Omega_m(X, Y)\nabla \cdot \big(K(X, Y)\nabla\Omega_n(X, Y)\big)dV \tag{9b}$$

$$c_{mn} = \omega_n^2\delta_{mn} \tag{9c}$$

$$e_{mn} = \int_V K_{\text{ac}}(X, Y)\Omega_m(X, Y)\Omega_n(X, Y)dV \tag{9d}$$

$$b_{mn} = \int_V U(X,Y)\Omega_m(X,Y)\Omega_n(X,Y)dV \tag{9e}$$

where δ_{mn} is the Kronecker delta.

Thus, the original eigenvalue problem given by Eq. (6a) has been reduced to the nonlinear algebraic eigenvalue problem given by Eq. (9a). In order to solve this equation, the following transformation is proposed [34]:

$$\xi^2\mathbf{G}\{\phi\} = \mathbf{H}\{\phi\} \tag{10a}$$

where the coefficient matrices are constructed as

$$\mathbf{G} = \begin{bmatrix} [\mathbf{0}] & [\boldsymbol{E}] \\ [\boldsymbol{E}] & [\boldsymbol{B}] \end{bmatrix}, \tag{10b}$$

$$\mathbf{H} = \begin{bmatrix} [\boldsymbol{E}] & [\mathbf{0}] \\ [\mathbf{0}] & [\boldsymbol{F}] \end{bmatrix}, \tag{10c}$$

$$\mathbf{F} = \mathbf{A} + \mathbf{C} \tag{10d}$$

The problem defined by Eq. (10a) is readily solvable with the *Mathematica* software system [35] and comes from the following decomposition of Eq. (9a):

$$\eta^2\mathbf{E}\{\phi_2\} = \mathbf{E}\{\phi_1\} \tag{10e}$$

$$\eta^2\mathbf{E}\{\phi_1\} + \eta^2\mathbf{B}\{\phi_2\} = \mathbf{F}\{\phi_2\} \tag{10f}$$

with:

$$\{\phi\} = \begin{pmatrix} \{\phi_1\} \\ \{\phi_2\} \end{pmatrix} \tag{10g}$$

Therefore, the sought eigenvectors $\{\bar{\psi}\}$ correspond to the calculated eigenvectors $\{\phi_2\}$ and their associated eigenvalues ξ^2 provide the values for the sought eigenvalues η^2. Then, Eq. (7b) is invoked to construct the desired eigenfunctions $\psi_i(X,Y)$.

In order to determine the coefficients C_i, $i = 1,\ldots,M$ in the truncated expansion in Eq. (5), we must make use of the entrance condition and the eigenfunctions orthogonality property, which can be obtained by manipulating Eq. (6a) and making use of the corresponding boundary conditions combined with Green's second identity, yielding:

$$\int_V [U(X,Y) + (\eta_i^2 + \eta_j^2)K_{ac}(X,Y)]\psi_j\psi_i dV = n_i\delta_{ij} \tag{11a}$$

$$n_i = \int_V [U(X,Y) + 2\eta_i^2 K_{ac}(X,Y)]\psi_i^2 dV \tag{11b}$$

where δ_{ij} is the Kronecker delta.

Now, we make use of the entrance condition $(Z = 0)$ expressed in terms of the solution given by the expansion in Eq. (5) truncated with N terms, as follows:

$$\theta^*(X,Y,0) = \sum_{i=1}^{N} C_i\psi_i(X,Y) \tag{12}$$

Operating on Eq. (4b) with $\int_V [U(X,Y) + \eta_j^2 K_{ac}(X,Y)]\psi_j(.)dV$, one obtains

$$\int_V [U(X,Y) + \eta_j^2 K_{ac}(X,Y)]\psi_j\theta^*(X,Y,0)dV = \sum_{i=1}^{N} C_i \int_V [U(X,Y) + \eta_j^2 K_{ac}(X,Y)]\psi_i\psi_j dV,\ j = 1,2,\ldots,N \tag{13}$$

Then, adding the term $\sum_{i=1}^{N} C_i \int_V \eta_i^2 K_{ac}(X,Y)\psi_i\psi_j dY$ at both sides of Eq. (13) and making use of the orthogonality property given by Eq. (11a), the following system can be written in terms of the unknowns C_i, $i = 1,\ldots,N$:

$$C_j n_j - \int_V [U(X,Y) + \eta_j^2 K_{ac}(X,Y)]\psi_j\theta^*(X,Y,0)dV - \sum_{i=1}^{N} C_i \int_V \eta_i^2 K_{ac}(X,Y)\psi_i\psi_j dV = 0,\ j = 1,2,\ldots,N \tag{14}$$

The system defined in Eq. (14) can be symbolically solved with the function *Solve* in the *Mathematica* platform [35], yielding the analytical expressions for C_i, $i = 1,\ldots,N$. Once this solution is made available, the expansion given by Eq. (5) can be readily evaluated, yielding the solution for θ^* at any position (X, Y, Z). Once the solution for the augmented domain is available, $\theta^*(X,Y,Z)$, the solution for the original domain, $\theta(X,Y,Z)$, can be readily obtained by simply suppressing the fictitious layer.

3 Inverse problem formulation and solution methodology

In the Bayesian framework, the inverse problem is formulated as a problem of statistical inference and is based on the following principles [36, 37]: (1) The parameters in the model are modeled as random variables; (2) the randomness describes our degree of information; (3) the degree of information is coded in probability distributions; and (4) the solution of the inverse problem is the posterior probability distribution. Thus, in the Bayesian approach all possible information is incorporated in the model in order to reduce the amount of uncertainty present in the problem to be solved.

The inverse analysis tackled in this work consists of determining some parameters appearing in the model, here denoted by the vector $\mathbf{P}$, employing a set of temperature measurements $\mathbf{Y}$. Consider that some prior information about the parameters can possibly be available. The Bayes' theorem for inverse problems can be expressed as [36, 37]:

$$\pi(\mathbf{P}|\mathbf{Y}) = \frac{\pi(\mathbf{P})\pi(\mathbf{Y}|\mathbf{P})}{\pi(\mathbf{Y})} \tag{15}$$

where $\pi(\mathbf{P}|\mathbf{Y})$ is the posterior probability density, $\pi(\mathbf{P})$ is the prior information on the unknowns, modeled as a probability distribution, $\pi(\mathbf{Y}|\mathbf{P})$ is the likelihood function, and $\pi(\mathbf{Y})$ is the marginal density, which plays the role of a normalizing constant.

Note that the statistical inverse method produces a distribution which may be explored in different ways, using different methods. In this work, we use the maximum a posteriori (MAP) estimator in order to produce single-point estimates for the parameters [37]. Consider that the prior information on the parameters can be modeled as a normal distribution. Thus, $\pi(\mathbf{P})$ can be expressed by

$$\pi(\mathbf{P}) = (2\pi)^{-N_p/2}|\mathbf{V}|^{1/2} \exp\left[-\frac{1}{2}(\mathbf{P}-\boldsymbol{\mu})^T\mathbf{V}^{-1}(\mathbf{P}-\boldsymbol{\mu})\right] \tag{16}$$

where N_p is the number of parameters, $\mathbf{V}$ and $\boldsymbol{\mu}$ are, respectively, the covariance matrix and the mean for $\mathbf{P}$, as modeled from the prior information. Furthermore, assuming that the experimental errors are additive, with zero mean, and following a normal distribution, the likelihood function can be expressed as:

$$\pi(\mathbf{Y}|\mathbf{P}) = (2\pi)^{-N_d/2}|\mathbf{W}|^{-1/2} \exp\left\{-\frac{1}{2}[\mathbf{Y}-\boldsymbol{\theta}(\mathbf{P})]^T\mathbf{W}^{-1}[\mathbf{Y}-\boldsymbol{\theta}(\mathbf{P})]\right\} \tag{17}$$

where N_d is the total number of experimental data available, $\mathbf{W}$ is the covariance matrix of the experimental errors, and $\boldsymbol{\theta}(\mathbf{P})$ is the vector of calculated temperatures at the same positions where the measured temperatures $\hat{e}(\mathbf{Y})$ are available. Substituting Eqs. (16) and (17) into Eq. (15) and taking the logarithm yields:

$$\ln[\pi(\mathbf{P}|\mathbf{Y})] \propto -\frac{1}{2}\left[(N_p+N_d)\ln(2\pi) + \ln|\mathbf{W}| + \ln|\mathbf{V}| + S(\mathbf{P})\right] \tag{18}$$

where

$$S(\mathbf{P}) = [\mathbf{Y}-\boldsymbol{\theta}(\mathbf{P})]^T\mathbf{W}^{-1}[\mathbf{Y}-\boldsymbol{\theta}(\mathbf{P})] + [\mathbf{P}-\boldsymbol{\mu}]^T\mathbf{V}^{-1}[\mathbf{P}-\boldsymbol{\mu}] \tag{19}$$

is the maximum a posteriori (MAP) objective function. The minimization of $S(\mathbf{P})$ yields the estimates $\mathbf{P}$ which maximize the posterior distribution $\pi(\mathbf{P}|\mathbf{Y})$. In this work, the MAP objective function is minimized with the iterative procedure of the Gauss–Newton method [38, 39]

$$\mathbf{P}^{n+1} = \mathbf{P}^n + [\mathbf{J}^T\mathbf{W}^{-1}\mathbf{J}+\mathbf{V}^{-1}]^{-1}[\mathbf{J}^T\mathbf{W}^{-1}(\mathbf{Y}-\boldsymbol{\theta}(\mathbf{P}^n)) + \mathbf{V}^{-1}(\boldsymbol{\mu}-\mathbf{P}^n)] \tag{20}$$

The elements of the Jacobian matrix $\mathbf{J}$ are given by

$$J_{ij} = \frac{\partial\theta_i(\mathbf{P})}{\partial P_j},\ i=1,2,\dots,N_d,\ j=1,2,\dots,N_p \tag{21}$$

For normally distributed measurement errors with zero mean and constant variance, the standard deviation of the estimated parameters corresponding to the maximum a posteriori objective function can be approximated from the expression [39]

$$\sigma_{P_i} = \sqrt{[(\mathbf{J}^T\mathbf{W}^{-1}\mathbf{J}+\mathbf{V}^{-1})^{-1}]_{i,i}},\ i=1,2,\dots,N_p \tag{22}$$

Assuming a normal distribution for measurement errors and 95% confidence, the bounds for the estimated quantities $\hat{P}_i$ are determined as:

$$\hat{P}_i^- = \hat{P}_i - 1,96\sigma_{P_i}, \tag{23a}$$

$$\hat{P}_i^+ = \hat{P}_i + 1,96\sigma_{P_i},\ i=1,2,\dots,N_p \tag{23b}$$

The sensitivity analysis plays a major role in several aspects related to the formulation and solution of inverse problems [38]. The elements of the sensitivity matrix $\mathbf{J}$, defined in Eq. (21), are called the sensitivity coefficients. In order to obtain good estimates, within reasonable confidence bounds, it is required that the sensitivity coefficients be high and, when two or more unknowns are estimated simultaneously, their sensitivity coefficients must be linearly independent. Otherwise, $|\mathbf{J}^T\mathbf{J}| \approx 0$ and the problem is ill-conditioned. In this work, for the sensitivity analysis, the scaled sensitivity coefficients are used:

$$\mathcal{J}_{ij} = P_j J_{ij},\ i=1,2,\dots,N_d,\ j=1,2,\dots,N_p \tag{24}$$

4 Results and discussion

The limiting situation of a rectangular channel with high aspect ratio is considered for numerical computations, in which $L_x >> L_y$ and, thus, the transversal direction X is neglected, so as to reduce the number of parameters in the analysis. It is considered that the external face of the channel wall exchanges heat with the surrounding environment, at T_∞, different from the inlet gas temperature (T_{in}), with a heat transfer coefficient h_e. The channel wall is considered to participate in the heat transfer process through axial and transversal heat conduction. The fluid enters the channel with a fully developed velocity profile, $u_f(y)$, and with an inlet temperature, T_{in}. The single-domain representation of this problem is depicted in Fig. 2.

The thickness and thermal conductivity of the fictitious layer, ϵ_{fic} and K_{fic}, respectively, are chosen so as to impose the desired thermal resistance to model the temperature jump. So, for this case, we must have:

$$\theta^*(Y_{int} + \epsilon_{fic}, Z) - \theta^*(Y_{int}, Z) = 2\mathrm{Kn}\beta_t \left.\frac{\partial \theta^*}{\partial Y}\right|_{Y=Y_{int}} \tag{25}$$

The heat flux across the fictitious layer can be written as:

$$-K_{fic} \left.\frac{\partial \theta^*}{\partial Y}\right|_{Y=Y_{int}} = \frac{\theta^*(Y_{int}, Z) - \theta^*(Y_{int} + \epsilon_{fic}, Z)}{\epsilon_{fic}/K_{fic}} \tag{26}$$

Substituting Eq. (26) into Eq. (25) readily yields:

$$\frac{\epsilon_{fic}}{K_{fic}} = 2\mathrm{Kn}\beta_t \tag{27}$$

Hence, the fictitious layer introduced can be set with arbitrary values for the dimensionless thickness and thermal conductivity in such a way that the ratio given by Eq. (27) is satisfied for the given values of Kn and β_t.

The wall temperature jump coefficient is given by [31]:

$$\beta_t = \frac{(2-\alpha_t)}{\alpha_t}\frac{2\gamma}{(\gamma+1)}\frac{1}{\mathrm{Pr}} \tag{28}$$

where α_t is the thermal accommodation coefficient and $\gamma = c_p/c_v$ is the specific heat ratio.

The dimensionless velocity profile for the high aspect ratio channel can be written as [13]:

$$U_f(Y) = \frac{6\mathrm{Kn}\beta_v + 3(1-Y^2)/2}{1 + 6\mathrm{Kn}\beta_v} \tag{29}$$

where

$$\beta_v = \frac{2-\alpha_m}{\alpha_m} \tag{30}$$

is the wall velocity slip coefficient and α_m is the tangential momentum accommodation coefficient.

The inverse analysis tackled in this work consists of determining the values of the following parameters: wall temperature jump coefficient, β_t, wall velocity slip coefficient, β_v, and Biot number, Bi, in different possible experimental setups.

The numerical results here presented consider the dimensionless thermal conductivity calculated as motivated by an application with a microchannel made of PMMA (polymethyl methacrylate), with $k_s = 0.2$ W/mK, with air as the working fluid, $k_f = 0.0271$ W/mK, so that $K_s = k_s/k_f = 7.38$. The following typical values were adopted for the governing parameters [31]: $\beta_t = 2$, $\beta_v = 1.5$, Kn = 0.0025, 0.0095, and 0.025, and Bi = 1, 5, and 10. As the thickness of the fictitious layer it was adopted $\epsilon_{fic} = 0.05$, and K_{fic} was calculated accordingly so as to satisfy Eq. (27) for the desired values of β_t and Kn. In all simulations, it was considered Pe = 1, as low Péclet numbers are the most commonly encountered cases in microscale applications.

Initially, a convergence analysis of the solution is presented for different truncation orders (N) in the eigenfunction expansion of the calculated temperatures, Eq. (5),

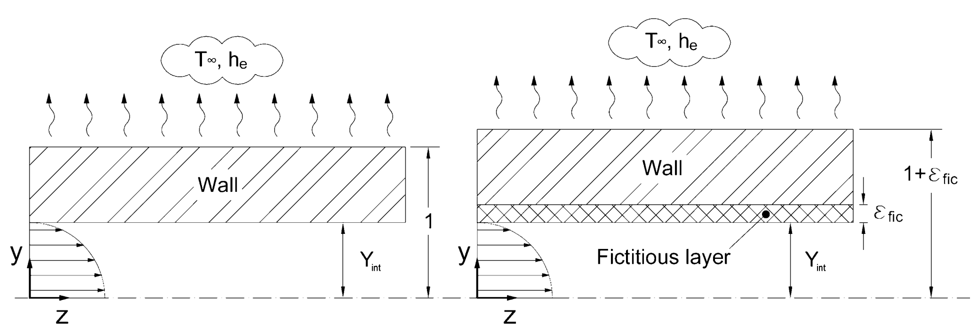

Fig. 2 Schematic representation of the original domain (left) and the augmented domain (right)

Table 1 Convergence behavior of the calculated temperatures for different truncation orders in the eigenfunction expansion (N), with $M = 200$ terms, Kn = 0.025, and $Y_{int} = 1$ (no conjugation effects)

N	Bi = 1		Bi = 5		Bi = 10	
	$\theta(0, 0.05)$	$\theta(0.25, 0.75)$	$\theta(0, 0.05)$	$\theta(0.25, 0.75)$	$\theta(0, 0.05)$	$\theta(0.25, 0.75)$
5	0.98099	0.62665	0.98034	0.53069	0.98201	0.50925
10	0.97950	0.62768	0.97278	0.53172	0.97103	0.51028
15	0.97988	0.62774	0.97393	0.53178	0.97268	0.51034
20	0.97984	0.62775	0.97373	0.53179	0.97238	0.51035
25	0.97986	0.62775	0.97379	0.53180	0.97247	0.51036
30	0.97986	0.62775	0.97378	0.53180	0.97245	0.51036

while keeping fixed the truncation order (M) employed in the solution of the non-classical eigenvalue problem with spatially varying coefficients, Eq. (7b). Tables 1 and 2 present the convergence behavior of the calculated temperatures for the case with no conjugation effects ($Y_{int} = 1$) and for the conjugated heat transfer problem case (with $Y_{int} = 0.5$), respectively, at two selected positions, for different Biot and Knudsen numbers, with N ranging from $N = 5$ to $N = 30$, and $M = 200$ terms in the eigenvalue problem solution. These results show a consistent convergence of at least four significant digits for $N \leq 25$. With only $N = 10$ terms, the results are already essentially converged to the third significant digit. It is also worth noting that the convergence behavior regarding the conjugated problem is as good as the case with no conjugation effects.

The convergence analysis of the solution is also presented for different truncation orders (M) regarding the eigenfunction expansions employed in solution of the non-classical eigenvalue problem, Eq. (7b), while keeping fixed the truncation order employed in the calculated temperatures, with $N = 30$ terms, which is enough to achieve convergence of the fourth significant digit, as demonstrated in Tables 1 and 2. First, Table 3 shows the calculated temperatures for the case with no conjugation effects ($Y_{int} = 1$) in two different transversal positions: $Y = 0$ (channel center) and $Y = 0.5$, and two different positions over the channel length: $Z = 0.05$ and $Z = 1.50$, for truncation orders ranging from $M = 50$ to $M = 200$. The results presented are converged with three to four significant digits for $M \leq 200$. A more cumbersome case is investigated in Tables 4 and 5, as the conjugated heat transfer problem case is presented (with $Y_{int} = 0.5$) for different Knudsen numbers. Table 4 illustrates the convergence of the calculated temperatures at the fluid region, whereas Table 5 illustrates the convergence of the calculated temperatures at the wall region. As the abrupt transitions in the spatially varying coefficients that represent the two different

Table 2 Convergence behavior of the calculated temperatures for different truncation orders in the eigenfunction expansion (N), with $M = 200$ terms, Bi = 10, and $Y_{int} = 0.5$ (conjugated problem)

N	Kn = 0.0025		Kn = 0.0095		Kn = 0.025	
	$\theta(0, 0.05)$	$\theta(0.25, 0.75)$	$\theta(0, 0.05)$	$\theta(0.25, 0.75)$	$\theta(0, 0.05)$	$\theta(0.25, 0.75)$
5	0.98280	0.51052	0.98669	0.52001	0.99317	0.54050
10	0.97312	0.51050	0.97380	0.51997	0.97514	0.54042
15	0.97383	0.51049	0.97443	0.51997	0.97542	0.54042
20	0.97354	0.51049	0.97410	0.51997	0.97531	0.54042
25	0.97358	0.51049	0.97412	0.51997	0.97531	0.54042
30	0.97356	0.51049	0.97411	0.51997	0.97531	0.54042

Table 3 Convergence behavior of the calculated temperatures for different truncation orders of the non-classical eigenvalue problem solution (M), with $N = 30$ terms, Kn = 0.025, and $Y_{int} = 1.0$ (no conjugation effects)

M	Bi = 1		Bi = 5		Bi = 10	
	$\theta(0, 0.05)$	$\theta(0.5, 1.50)$	$\theta(0, 0.05)$	$\theta(0.5, 1.50)$	$\theta(0, 0.05)$	$\theta(0.5, 1.50)$
50	0.97985	0.31701	0.97374	0.20362	0.97240	0.18215
75	0.97984	0.31720	0.97370	0.20399	0.97235	0.18258
100	0.97986	0.31722	0.97378	0.20402	0.97245	0.18261
125	0.97986	0.31729	0.97376	0.20416	0.97242	0.18277
150	0.97986	0.31730	0.97379	0.20419	0.97245	0.18279
175	0.97986	0.31732	0.97377	0.20423	0.97243	0.18285
200	0.97986	0.31734	0.97374	0.20427	0.97245	0.18289

Table 4 Convergence behavior of the calculated temperatures at the fluid region for different truncation orders of the non-classical eigenvalue problem solution (M), with $N = 30$ terms, Bi = 10, and $Y_{int} = 0.5$ (conjugated problem)

M	Kn = 0.0025		Kn = 0.0095		Kn = 0.025	
	$\theta(0, 0.05)$	$\theta(0.5, 1.50)$	$\theta(0, 0.05)$	$\theta(0.5, 1.50)$	$\theta(0, 0.05)$	$\theta(0.5, 1.50)$
50	0.97163	0.14195	0.97227	0.14908	0.97334	0.16475
75	0.97337	0.14846	0.97394	0.15576	0.97504	0.17227
100	0.97299	0.15206	0.97358	0.15951	0.97474	0.17686
125	0.97348	0.15434	0.97408	0.16184	0.97527	0.17956
150	0.97338	0.15592	0.97394	0.16348	0.97513	0.18140
175	0.97362	0.15707	0.97100	0.16231	0.97537	0.18280
200	0.97356	0.15793	0.97100	0.16231	0.97531	0.18380

Table 5 Convergence behavior of the calculated temperatures at the wall region for different truncation orders of the non-classical eigenvalue problem solution (M), with $N = 30$ terms, Bi = 10, and $Y_{\text{int}} = 0.5$ (conjugated problem)

M	Kn = 0.0025		Kn = 0.0095		Kn = 0.025	
	$\theta(0.5, 0.05)$	$\theta(1, 1.50)$	$\theta(0.5, 0.05)$	$\theta(1, 1.50)$	$\theta(0.5, 0.05)$	$\theta(1, 1.50)$
50	0.94841	0.08847	0.95031	0.08841	0.95314	0.08816
75	0.94850	0.09599	0.95041	0.09587	0.95418	0.09559
100	0.94940	0.10012	0.95167	0.10002	0.95553	0.09974
125	0.94958	0.10278	0.95160	0.10267	0.95558	0.10237
150	0.94983	0.10461	0.95211	0.10450	0.95620	0.10421
175	0.94999	0.10600	0.95211	0.10585	0.95609	0.10554
200	0.94993	0.10699	0.95230	0.10687	0.95649	0.10657

domains (fluid stream and channel wall) are considered in the eigenvalue problem, this case presents slightly slower convergence rates if compared to the case with no conjugation effects. Here, a convergence of two to three significant digits is observed. It should be highlighted that these results can be considered sufficiently accurate for the simulations and inverse analyses, once the maximum associated errors (in the order of 0.1%) are much smaller than the expected measurement errors.

Before addressing the estimation of the unknown parameters, a sensitivity analysis is shown, in order to give some insights regarding the influence of such parameters in the inverse problem solution. Based on possible experimental setups, three different wall Biot numbers are considered, Bi = 1, 5, and 10, for the problem with no conjugation effects, i.e., $Y_{\text{int}} = 1.0$, considering Kn = 0.025. Figure 3a–c depicts the scaled sensitivity coefficients with respect to the parameters β_t, β_v, and Bi, respectively. It should be noticed that increasing the Biot number increases the sensitivity for β_t, but decreases the sensitivity for β_v and Bi. Besides, it should be observed that the sensitivity coefficients with respect to β_t and Bi are linearly dependent, as already observed in [31]. Nevertheless, prior information can actually be obtained for Bi, for example from empirical correlations for external convection, and also for β_v, by utilizing pressure and mass flow rate measurements for an initial estimate of the slip coefficient. In this context, higher values of the Biot number can possibly benefit this inverse problem solution regarding the estimation of β_t if good prior information for β_v and Bi is available, despite an overall reduction in $|\mathbf{J}^T\mathbf{J}|$, which was pointed out in [31].

Another possibility brought by the model proposed in this work, which takes into account the wall conjugation effects, is the evaluation of different experimental setups based on the thickness of the channel wall. Figure 4a–c depicts the scaled sensitivity coefficients with respect to the parameters β_t, β_v, and Bi, respectively, for three different wall thickness values, $Y_{\text{int}} = 1.0$ (no conjugation), $Y_{\text{int}} = 0.5$, and $Y_{\text{int}} = 0.25$, considering Bi = 10 and Kn = 0.025. Once again, it can be noticed that the sensitivity with respect to β_t and Bi presents opposite behaviors: Increasing the channel thickness increases the sensitivity to Bi, but decreases the sensitivity to β_t.

As Knudsen numbers in the range $10^{-3} < \text{Kn} < 10^{-1}$ are often found in microsystems [33], an evaluation of different experimental setups based on the Knudsen number is also performed. Figure 5a–c depicts the scaled sensitivity coefficients with respect to the parameters β_t, β_v, and Bi, respectively, for three different Knudsen numbers, Kn = 0.0025, Kn = 0.0095, and Kn = 0.025, for the conjugated heat conduction problem in which $Y_{\text{int}} = 0.5$, considering Bi = 10. It can be noticed that increasing the Knudsen number increases the sensitivity to β_t, the main parameter to be estimated in the inverse problem. It is important to highlight that although the sensitivity to Bi is relatively high, it is little affected by the Knudsen number.

For the numerical examples regarding the inverse problem solution, to be presented next, only external wall temperature measurements are considered in this work, which could be obtained with an infrared measurements system, for example [40]. The experimental data $\mathbf{Y}$ have been simulated by calculating the temperature distribution with the model proposed, after which random noise from a normal distribution has been added:

$$Y_i = \theta_i(\mathbf{P}_{\text{exact}}) + \sigma_e r_i,\ i = 1, 2, \ldots, N_d \tag{31}$$

where r_i are random numbers drawn from a normal distribution with zero mean and unitary standard deviation. A total of 200 uniformly distributed points along the channel length from $Z = 0$ to $Z = Z_f = 2$ were considered. In order to alleviate the effects of the inverse crime [36], the experimental data have been simulated employing a solution with truncation orders $N = 30$ and $M = 200$, while the direct problem solution within the inverse problem procedure was handled with $N = 10$ and $M = 50$ terms.

Once the sensitivity coefficients regarding the Biot number (Bi) and the wall temperature jump coefficient (β_t) are linearly correlated, and prior information is available for Bi, some numerical test cases are proposed next, in order to evaluate the effects of these possible experimental setups on the estimated parameters. Table 6 presents the estimates

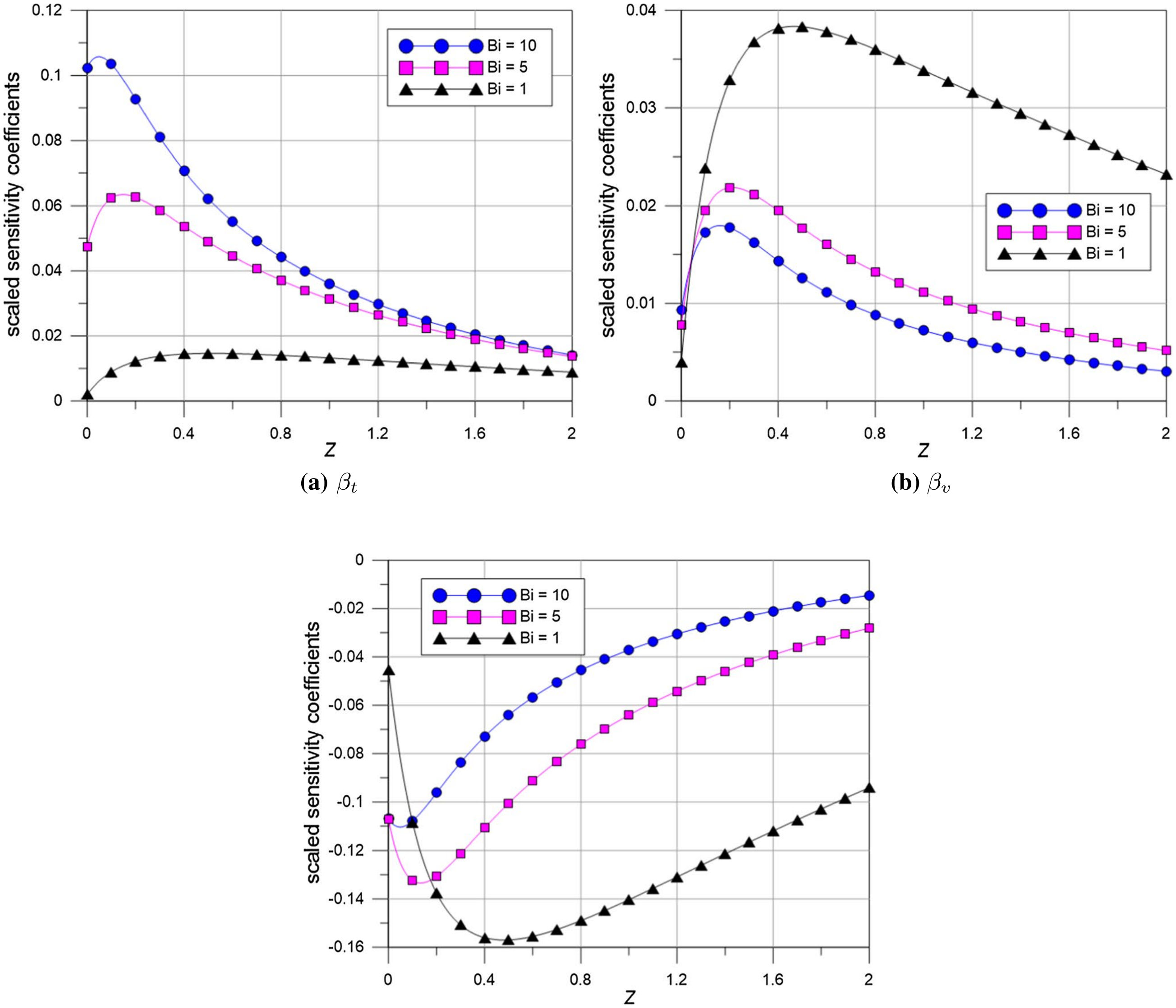

(a) β_t

(b) β_v

(c) Bi

Fig. 3 Scaled sensitivity coefficients for different wall Biot numbers: Bi = 10, Bi = 5, and Bi = 1, considering $Y_{\text{int}} = 1.0$ and Kn = 0.025

obtained for the case with no conjugation effects ($Y_{\text{int}} = 1.0$) for different wall Biot numbers, Bi = 1, 5, and 10. In these cases, $\sigma_e = 0.0025$ was considered in Eq. (31) to model the experimental errors. Prior information for β_v and Bi can be obtained, for instance by utilizing pressure and mass flow rate measurements to approximate the slip coefficient and by employing classical correlations for estimating the external heat transfer coefficient, respectively. Then, the a priori information for β_v and Bi was modeled as independent Gaussian distributions with means at the exact values and standard deviations of 10% and 12.5% of their means, respectively. For β_t, it was initially considered a much less informative prior, also modeled as a Gaussian distribution with 1.5 mean (it should be recalled that the exact value is 2.0, supposedly unknown) with standard deviation of 67% of the mean. In order to allow for a direct comparison between different cases, it is also presented in the tables a relative measure of the confidence intervals range, given by:

$$CI_i = \frac{\hat{P}_i^+ - \hat{P}_i^-}{P_{i,\text{exact}}},\ i = 1, 2, \dots, N_p \tag{32}$$

where $\hat{P}_i^+$ is the upper limit of the estimated confidence interval regarding the parameter estimate $\hat{P}_i$, $\hat{P}_i^-$ is the lower limit, and $P_{i,\text{exact}}$ is the exact parameter value.

In Table 6, it can be observed, as already previewed in the sensitivity analysis, that the estimation of Bi is indeed much more precise for Bi = 1 than for Bi = 10, but, on the other

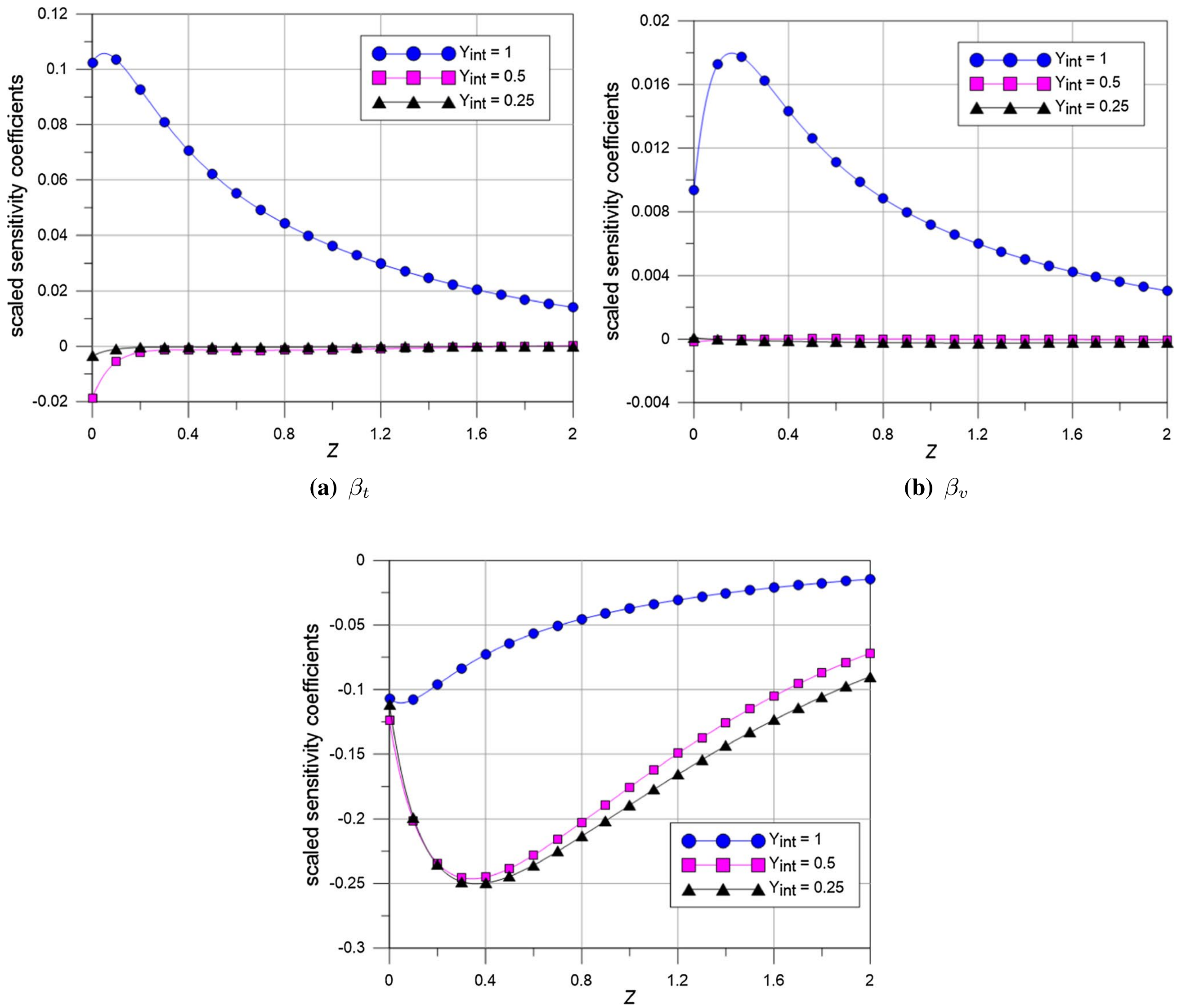

(a) β_t **(b)** β_v **(c)** Bi

Fig. 4 Scaled sensitivity coefficients for different wall thicknesses: $Y_{\text{int}} = 1.0$, $Y_{\text{int}} = 0.5$, and $Y_{\text{int}} = 0.25$, considering Bi = 10 and Kn = 0.025

hand, the estimation of β_t becomes significantly affected for decreasing Biot numbers.

In this context, a better estimation can still be tried by varying the channel wall thickness, recalling that for increasing wall thickness the sensitivity to Bi increases. Table 7 presents these results, demonstrating that when the wall thickness is increased a much better estimation can in fact be obtained for Bi. Regarding the parameter β_t, it is observed that for $Y_{\text{int}} = 0.5$ a more precise estimation is obtained in comparison with the case with no conjugation effects (probably as influence of the increase in quality of the estimated Biot number), whereas for $Y_{\text{int}} = 0.25$ a worse result is obtained. (In this case, the precision of the estimated Biot number does not increase anymore, and the estimation precision of β_t is still worse, as demonstrated in the sensitivity analysis.) These results suggest that there possibly exists an optimum channel wall thickness that maximizes the precision in the estimation of the temperature jump coefficient, β_t.

Another possibility to obtain a better estimation for the parameter β_t can still be tried by varying the Knudsen number. In Table 8, it can be observed, as anticipated in the sensitivity analysis, that the estimation of β_t is more precise for higher values of the Knudsen number, whereas the estimation of Bi is not significantly affected by variations of Kn.

Finally, in order to evaluate the consistency of the results obtained with respect to the experimental errors and the influence of the prior information given to the parameter β_t, a final

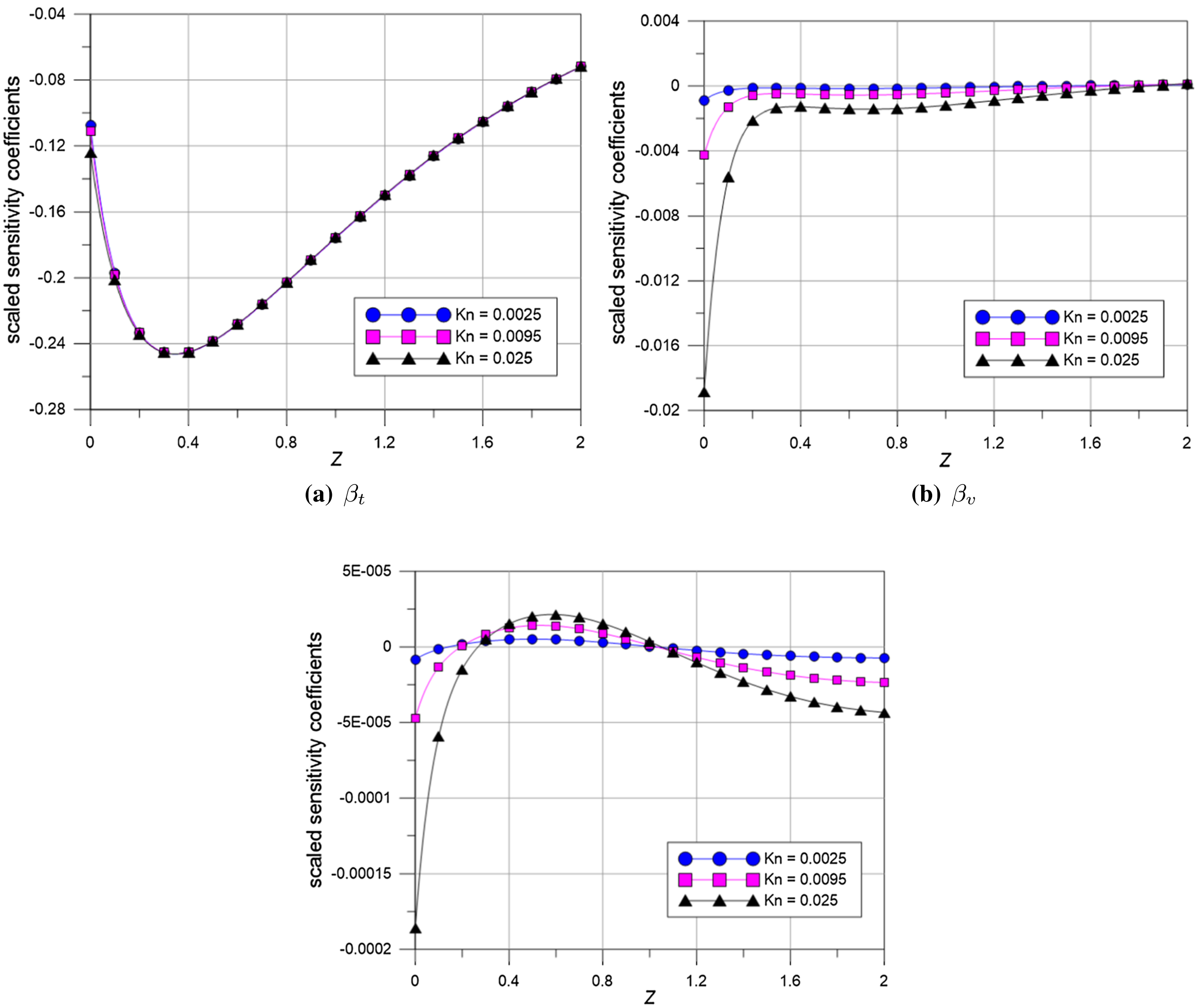

(a) β_t **(b)** β_v **(c)** Bi

Fig. 5 Scaled sensitivity coefficients for different Knudsen numbers: Kn = 0.0025, Kn = 0.0095, and Kn = 0.025, considering Bi = 10 and $Y_{\text{int}} = 0.5$

test is considered, in which $\sigma_e = 0.005$ (twice the previous noise level), and no prior information is considered available for β_t. These results are presented in Table 9, demonstrating that, in fact, no prior information is needed for β_t. The estimated confidence intervals are obviously wider than those presented in Table 6a as a result of higher experimental errors, but reasonable confidence intervals are still obtained.

5 Concluding remarks

The inverse analysis of forced internal convection with slip flow inside rectangular channels is investigated in this work, taking into account axial conduction and wall conjugation effects. For the direct problem solution, the generalized integral transform technique, combined with a single-domain formulation strategy, was employed. The inverse problem was formulated within the Bayesian framework in order to estimate the temperature jump coefficient, employing prior information for the velocity slip coefficient and wall Biot numbers and using only external temperature measurements along the channel wall. The results here reported investigated different possible experimental setups, suggesting that higher wall Biot numbers and higher Knudsen numbers (within the range of the slip flow regime) are favorable to the estimation of the temperature jump coefficient, as well as indicating the possible existence of an optimum channel wall

Table 6 Estimates obtained for the case with no conjugation effects and σ_e = 0.0025 for different possible experimental setups

Parameter	Prior	Estimate	Exact	95% conf. int.	CI_i
(a) Bi = 10					
β_t	*N*(1.5, 1)	1.92	2.00	[1.39, 2.45]	53%
β_v	*N*(1.5, 0.15)	1.50	1.50	[1.28, 1.73]	30%
Bi	*N*(10, 1.25)	9.59	10.00	[7.30, 11.8]	45%
(b) Bi = 5					
β_t	*N*(1.5, 1)	1.97	2.00	[1.21, 2.73]	76%
β_v	*N*(1.5, 0.15)	1.53	1.50	[1.27, 1.78]	34%
Bi	*N*(10, 1.25)	4.98	5.00	[4.13, 5.83]	34%
(c) Bi = 1					
β_t	*N*(1.5, 1)	1.54	2.00	[0.46, 2.63]	108%
β_v	*N*(1.5, 0.15)	1.52	1.50	[1.25, 1.79]	36%
Bi	*N*(10, 1.25)	0.98	1.00	[0.94, 1.03]	9%

Table 7 Estimates obtained for the conjugated problem with Bi = 10 and σ_e = 0.0025 for different possible experimental setups

Parameter	Prior	Estimate	Exact	95% conf. int.	CI_i
(a) Y_{int} = 0.5					
β_t	*N*(1.5, 1)	2.02	2.00	[1.75, 2.29]	27%
β_v	*N*(1.5, 0.15)	1.50	1.50	[1.21, 1.79]	39%
Bi	*N*(10, 1.25)	10.0	10.00	[9.98, 10.02]	0.4%
(b) Y_{int} = 0.25					
β_t	*N*(1.5, 1)	2.22	2.00	[1.20, 3.23]	101%
β_v	*N*(1.5, 0.15)	1.50	1.50	[1.21, 1.80]	39%
Bi	*N*(10, 1.25)	9.99	10.00	[9.97, 10.01]	0.4%

Table 8 Estimates obtained for the conjugated problem with Bi = 10 and σ_e = 0.0025 for different possible experimental setups, considering Y_{int} = 0.5

Parameter	Prior	Estimate	Exact	95% conf. int.	CI_i
(a) Kn = 0.0025					
β_t	*N*(1.5, 1)	1.89	2.00	[0.05, 3.74]	185%
β_v	*N*(1.5, 0.15)	1.50	1.50	[1.21, 1.79]	39%
Bi	*N*(10, 1.25)	10.01	10.00	[9.99, 10.03]	0.4%
(b) Kn = 0.0095					
β_t	*N*(1.5, 1)	1.97	2.00	[0.92, 3.01]	105%
β_v	*N*(1.5, 0.15)	1.50	1.50	[1.21, 1.79]	39%
Bi	*N*(10, 1.25)	10.01	10.00	[9.99, 10.03]	0.5%
(c) Kn = 0.025					
β_t	*N*(1.5, 1)	1.99	2.00	[1.72, 2.26]	27%
β_v	*N*(1.5, 0.15)	1.50	1.50	[1.21, 1.80]	39%
Bi	*N*(10, 1.25)	9.98	10.00	[9.96, 10.01]	0.5%

Table 9 Estimates obtained for the conjugated problem with Bi = 10, Kn = 0.025, Y_{int} = 0.5, and σ_e = 0.005

Parameter	Prior	Estimate	Exact	95% conf. int.	CI_i
β_t	None	1.93	2.00	[1.39, 2.48]	54%
β_v	*N*(1.5, 0.15)	1.50	1.50	[1.21, 1.80]	39%
Bi	*N*(10, 1.25)	9.99	10.00	[9.96, 10.04]	0.8%

thickness that maximizes the precision in the estimation of this parameter.

Since the applications dealing with microsystems in gas flows involve very low Reynolds numbers, as discussed more closely in [14], the entry lengths for hydrodynamic development (roughly $L_h = 0.05\mathrm{Re}D_h$) are in general very small, of the order of a fraction of the channel hydraulic diameter, also very small due to the microchannel cross section dimensions. These lengths are in general negligible in comparison with the overall length of the microsystem [14], which justifies the adoption of the hydrodynamically developed flow assumption. Nevertheless, if required in a specific application, the present approach could be readily extended to the simultaneously developing flow situation, as previously employed in no-slip flow conditions [41]. Also, one may seek the extension of the present methodology to handle longitudinally variable heat transfer coefficients, such as in external forced convection along the channel wall or natural convection along vertical or inclined plates. References [40, 42, 43] illustrate the successful application of the GITT and MCMC combination in dealing with the direct and inverse analyses for conduction problems and convective boundary conditions with space variable heat transfer coefficients. Although this would certainly be an interesting extension to the present problem, the central focus in this contribution was the estimation of the slip flow and temperature jump parameters, and how the wall conjugation and axial diffusion effects would affect the reliability of these computations. As microsystems are usually of the order of a few centimeters at most, a marked spatial variation of the external heat transfer coefficient is not expected that could impact the estimation accuracy or add difficulties to the incorporation of such an effect. Nevertheless, in the methodology proposed for the estimation problem, we consider that prior information is available for the Biot number. In the numerical results presented, we considered just average Biot numbers that clearly allow to inspect the influence of the external convection coefficient magnitude on the quality of the estimates.

Acknowledgements This study was financed in part by CAPES—Coordenação de Aperfeiçoamento de Pessoal de Nível

Superior—Brasil, Finance Code 001. The authors would also like to thank the other sponsoring agencies, CNPq—Conselho Nacional de Desenvolvimento Científico e Tecnológico, and FAPERJ—Fundação Carlos Chagas Filho de Amparo à Pesquisa do Estado do Rio de Janeiro.

References

1. Sobhan CB, Peterson GP (2008) Microscale and nanoscale heat transfer: fundamentals and engineering applications. CRC Press, Boca Raton
2. Morini GL (2004) Single-phase convective heat transfer in microchannels: a review of experimental results. Int J Therm Sci 43(7):631–651
3. Rosa P, Karayiannis TG, Collins MW (2009) Single-phase heat transfer in microchannels: the importance of scaling effects. Appl Therm Eng 29(17–18):3447–3468
4. Zhang W-M, Meng G, Wei X (2012) A review on slip models for gas microflows. Microfluid Nanofluid 13(6):845–882
5. Ameel TA, Wang X, Barron RF, Warrington RO (1997) Laminar forced convection in a circular tube with constant heat flux and slip flow. Microscale Thermophys Eng 1(4):303–320
6. Larrodé FE, Housiadas C, Drossinos Y (2000) Slip-flow heat transfer in circular tubes. Int J Heat Mass Transf 43(15):2669–2680
7. Tunc G, Bayazitoglu Y (2001) Heat transfer in microtubes with viscous dissipation. Int J Heat Mass Transf 44(13):2395–2403
8. Hooman K, Ejlali A (2010) Effects of viscous heating, fluid property variation, velocity slip, and temperature jump on convection through parallel plate and circular microchannels. Int Commun Heat Mass Transf 37(1):34–38
9. Xiao N, Elsnab J, Ameel T (2009) Microtube gas flows with second-order slip flow and temperature jump boundary conditions. Int J Therm Sci 48(2):243–251
10. Norouzi M, Rezaie MR (2018) An exact analysis on heat convection of nonlinear viscoelastic flows in isothermal microtubes under slip boundary condition. J Braz Soc Mech Sci Eng 40(9):472
11. Yu S, Ameel TA (2001) Slip-flow heat transfer in rectangular microchannels. Int J Heat Mass Transf 44(22):4225–4234
12. Tunc G, Bayazitoglu Y (2002) Heat transfer in rectangular microchannels. Int J Heat Mass Transf 45(4):765–773
13. Mikhailov MD, Cotta RM (2005) Mixed symbolic-numerical computation of convective heat transfer with slip flow in microchannels. Int Commun Heat Mass Transf 32(3–4):341–348
14. Cotta RM, Knupp DC, Naveira-Cotta CP (2016) Analytical heat and fluid flow in microchannels and microsystems. Springer, Berlin
15. Renksizbulut M, Niazmand H, Tercan G (2006) Slip-flow and heat transfer in rectangular microchannels with constant wall temperature. Int J Therm Sci 45(9):870–881
16. Kuddusi L (2007) Prediction of temperature distribution and nusselt number in rectangular microchannels at wall slip condition for all versions of constant wall temperature. Int J Therm Sci 46(10):998–1010
17. Siginer DA, Akyildiz FT, Boutaous M (2019) Unsteady gaseous poiseuille slip flow in rectangular microchannels. J Braz Soc Mech Sci Eng 41(7):286
18. Maranzana G, Perry I, Maillet D (2004) Mini-and micro-channels: influence of axial conduction in the walls. Int J Heat Mass Transf 47(17–18):3993–4004
19. Nunes JS, Cotta RM, Avelino MR, Kakaç S (2010) Conjugated heat transfer in microchannels. In: Kakaç S, Kosoy B, Li D, Pramuanjaroenkij A (eds) Microfluidics based microsystems. NATO science for peace and security series A: chemistry and biology. Springer, Dordrecht
20. Maranzana G, Perry I, Maillet D (2004) Modeling of conjugate heat transfer between parallel plates separated by a hydrodynamically developed laminar flow by the quadrupole method. Numer Heat Transf Part A 46(2):147–165
21. Knupp DC, Cotta RM, Naveira-Cotta CP, Kakaç S (2015) Transient conjugated heat transfer in microchannels: integral transforms with single domain formulation. Int J Therm Sci 88:248–257
22. Knupp DC, Naveira-Cotta CP, Renfer A, Tiwari MK, Cotta RM, Poulikakos D (2015) Analysis of conjugated heat transfer in micro-heat exchangers via integral transforms and non-intrusive optical techniques. Int J Numer Methods Heat Fluid Flow 25(6):1444–1462. https://doi.org/10.1108/HFF-08-2014-0259
23. Knupp DC, Naveira-Cotta CP, Cotta RM (2014) Theoretical-experimental analysis of conjugated heat transfer in nanocomposite heat spreaders with multiple microchannels. Int J Heat Mass Transf 74:306–318
24. Knupp DC, Cotta RM, Naveira-Cotta CP (2015) Fluid flow and conjugated heat transfer in arbitrarily shaped channels via single domain formulation and integral transforms. Int J Heat Mass Transf 82:479–489
25. Souza J R B, Lisboa K M, Allahyarzadeh A B, de Andrade G J A, Loureiro J B R, Naveira-Cotta C P, Silva Freire A P, Orlande H R B, Silva G A L, Cotta R M (2016) Thermal analysis of anti-icing systems in aeronautical velocity sensors and structures. J Braz Soc Mech Sci Eng 38(5):1489–1509
26. Knupp DC, Mascouto FS, Abreu LAS, Naveira-Cotta CP, Cotta RM (2018) Conjugated heat transfer in circular microchannels with slip flow and axial diffusion effects. Int Commun Heat Mass Transf 91:225–233
27. Agrawal A, Prabhu SV (2008) Survey on measurement of tangential momentum accommodation coefficient. J Vac Sci Technol A Vac Surf Films 26(4):634–645
28. Rader DJ, Castaneda JN, Torczynski JR, Grasser TW, Trott WM (2005) Measurements of thermal accommodation coefficients. Technical report, Sandia National Laboratories
29. Sharipov F (2011) Data on the velocity slip and temperature jump on a gas-solid interface. J Phys Chem Ref Data 40(2):023101
30. McCormick NJ (2005) Gas-surface accommodation coefficients from viscous slip and temperature jump coefficients. Phys Fluids 17(10):107104
31. Naveira-Cotta CP, Cotta RM, Orlande HRB (2010) Inverse analysis of forced convection in micro-channels with slip flow via integral transforms and bayesian inference. Int J Therm Sci 49(6):879–888
32. Naveira-Cotta CP (2016) Direct-inverse problem analysis in the thermal characterization of microsystems. In: Rebay M, Kakaç S, Cotta RM (eds) Microscale and nanoscale heat transfer: analysis, design, and application. CRC Press, Boca Raton
33. Colin S (2012) Gas microflows in the slip flow regime: a critical review on convective heat transfer. J Heat Transf 134(2):020908
34. Knupp DC, Naveira-Cotta CP, Cotta RM (2013) Conjugated convection-conduction analysis in microchannels with axial diffusion effects and a single domain formulation. J Heat Transf 135(9):091401
35. Wolfram S et al (1996) Mathematica. Cambridge University Press, Cambridge
36. Kaipio J, Somersalo E (2006) Statistical and computational inverse problems, vol 160. Springer, Berlin
37. Orlande HRB, Fudym O, Maillet D, Cotta RM (2011) Thermal measurements and inverse techniques. CRC Press, Boca Raton
38. Özişik MN, Orlande HRB (2000) Inverse heat transfer: fundamentals and applications. CRC Press, Boca Raton

39. Beck JV, Arnold KJ (1977) Parameter estimation in engineering and science. James Beck, Denver
40. Knupp DC, Naveira-Cotta CP, Ayres JVC, Cotta RM, Orlande HRB (2012) Theoretical-experimental analysis of heat transfer in nonhomogeneous solids via improved lumped formulation, integral transforms and infrared thermography. Int J Therm Sci 62:71–84
41. Figueira da Silva E, Cotta RM (1996) Benchmark results for internal forced convection through integral transformation. Int Commun Heat Mass Transf 23(7):1019–1029
42. Knupp DC, Naveira-Cotta CP, Ayres JVC, Orlande HRB, Cotta RM (2012) Space-variable thermophysical properties identification in nanocomposites via integral transforms, bayesian inference and infrared thermography. Inverse Probl Sci Eng 20(5):609–637
43. Knupp DC, Naveira-Cotta CP, Orlande HRB, Cotta RM (2013) Experimental identification of thermophysical properties in heterogeneous materials with integral transformation of temperature measurements from infrared thermography. Exp Heat Transf 26(1):1–25